Coral Reefs (2004) 23: 48–59
DOI 10.1007/s00338-003-0365-7

REPORT

John C. Brock · C. Wayne Wright
Tonya D. Clayton · Amar Nayegandhi

LIDAR optical rugosity of coral reefs in Biscayne National Park, Florida

Received: 18 February 2003 / Accepted: 9 June 2003 / Published online: 4 February 2004

Abstract The NASA Experimental Advanced Airborne Research Lidar (EAARL), a temporal waveform-resolving, airborne, green wavelength LIDAR (light detection and ranging), is designed to measure the submeter-scale topography of shallow reef substrates. Topographic variability is a prime component of habitat complexity, an ecological factor that both expresses and controls the abundance and distribution of many reef organisms. Following the acquisition of EAARL coverage over both mid-platform patch reefs and shelf-margin bank reefs within Biscayne National Park in August 2002, EAARL-based optical indices of topographic variability were evaluated at 15 patch reef and bank reef sites. Several sites were selected to match reefs previously evaluated in situ along underwater video and belt transects. The analysis used large populations of submarine topographic transects derived from the examination of closely spaced laser spot reflections along LIDAR raster scans. At all 15 sites, each LIDAR transect was evaluated separately to determine optical rugosity (Ro_{tran}), and the average elevation difference between adjacent points ($Av(\delta E_{ap})$). Further, the *whole-site* mean and maximum values of Ro_{tran} and $Av(\delta E_{ap})$ for the entire population of transects at each analysis site, along with their standard deviations, were calculated. This study revealed that the greater habitat complexity of inshore patch reefs versus outer bank reefs results in relative differences in topographic complexity that can be discerned in the laser returns. Accordingly, LIDAR sensing of optical rugosity is proposed as a complementary new technique for the rapid assessment of shallow coral reefs.

J. C. Brock (✉) · T. D. Clayton · A. Nayegandhi
USGS Center for Coastal and Watershed Studies,
600 4th Street South, St. Petersburg, Florida 33701, USA
E-mail: jbrock@usgs.gov
Tel.: +1-727-803-8747
Fax: +1-727-803-2032

C. W. Wright
NASA Goddard Space Flight Center, Wallops Flight Facility,
Wallops Island, Virginia 23337, USA

Keywords Aircraft remote sensing · LIDAR · Rugosity · Monitoring · Florida Keys

Introduction

Variability in vertical relief, or rugosity, is a significant aspect of habitat complexity, a factor that both reflects and governs the spatial distribution and density of many reef organisms (Sale 1991; Sebens 1991; McCormick 1994). Topographic complexity on coral reefs is typically assessed along rugosity transects as the ratio of the horizontal distance crossed by a chain laid upon the reef surface contour to the linear horizontal distance between the two endpoints (Aronson et al. 1994; Rogers et al. 1994). Rugosity surveys are useful in studies of reef ecological structure and function (Sebens 1991; McCormick 1994; Szmant 1997), catastrophic change due to hurricane impacts and ship groundings (Rogers et al. 1982; Rogers and Miller 2001), long-term cumulative disturbance or bioerosion (Sebens 1991; Aronson et al. 1994), fish assemblage structure (Sale 1991; Hixon and Beets 1993; Friedlander and Parrish 1998), and associated conservation value (Chapman and Kramer 1999; Edinger and Risk 2000).

Most optical remote-sensing investigations of coral reefs involve the use of *passive* techniques that rely upon reflected sunlight (Mazel 1999). This class of remote sensing can be used to survey coarse bathymetry (Lyzenga 1978; Sandidge and Holyer 1998), but cannot capture the fine-scale morphology that is evaluated by measuring rugosity transects across reefs. An *active* remote-sensing approach utilizing a laser light source provides greater promise for sounding the detailed topography of shallow coral reefs. The LIDAR (light detection and ranging) altimeter deployed in this investigation is the Experimental Advanced Airborne Research Lidar (EAARL), a temporal waveform-resolving, green laser altimeter constructed at NASA

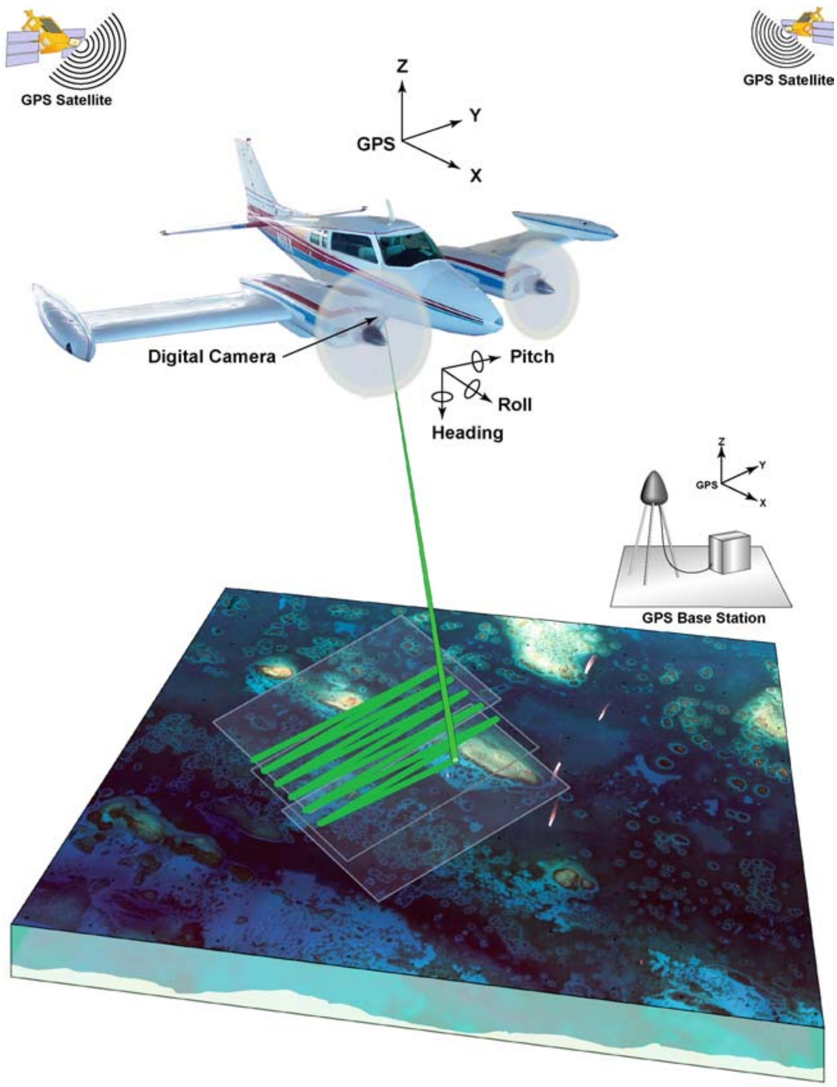

Fig. 1 The NASA Experimental Advanced Airborne Research Lidar (EAARL). Geolocation information is provided by kinematic differential GPS. Digital aerial photography is collected coincident with the laser scans

by one of the authors (C.W. Wright; Fig. 1). The first NASA EAARL surveys of a coral reef tract were carried out in the northern Florida Keys during the summers of 2001 and 2002, in parallel with in situ optical measurements and benthic cover assessments by SCUBA divers.

The goal of this study is to examine the capability of a temporal waveform-resolving, airborne green LIDAR to retrieve ecologically meaningful morphological information over shallow coral reef substrates. The specific objectives of this paper are to:

1. Describe the lineage and design of the EAARL, a new type of airborne LIDAR instrument that has capabilities for surveying the submeter-scale topographic complexity of shallow coral reefs.
2. Demonstrate the capability of small-footprint, temporal waveform-resolving, airborne green LIDAR to optically sense rugosity variation between reefs in Biscayne National Park (BNP) that are known to vary in habitat complexity.

Methods

Study area

The study area lies within Biscayne National Park on the northern margin of the Florida reef tract (Fig. 2a), a high-latitude reef system where both natural and anthropogenic impacts are severe (Johannes et al. 1983; Hudson et al. 1994). Relatively frequent hurricanes and cold-water disturbances combined with suspended sediment influx, eutrophication, and heavy recreational use exert stresses on the reef ecosystem (Burns 1985; Dustan 1999). Biscayne National Park covers the northern portion of a region of numerous patch reefs, transitional reefs, and platform-margin reefs that preferentially occur seaward of Elliott Key and Key Largo, islands underlain by Pleistocene limestone (Ginsburg and Shinn 1994).

The study area is on a carbonate platform situated seaward of Caesar's Creek, and bounded by Hawk Channel to the west and oceanward by the shelf edge (Fig. 2b). The landward portion of the study area is covered by carbonate sand, turtle grass, and numerous scattered patch reefs surrounded by bare sandy halos. On the shelf edge, discontinuous linear bank reefs capped mostly by coral rubble and sand are found (Shinn et al. 1989; McPherson and Halley 1996).

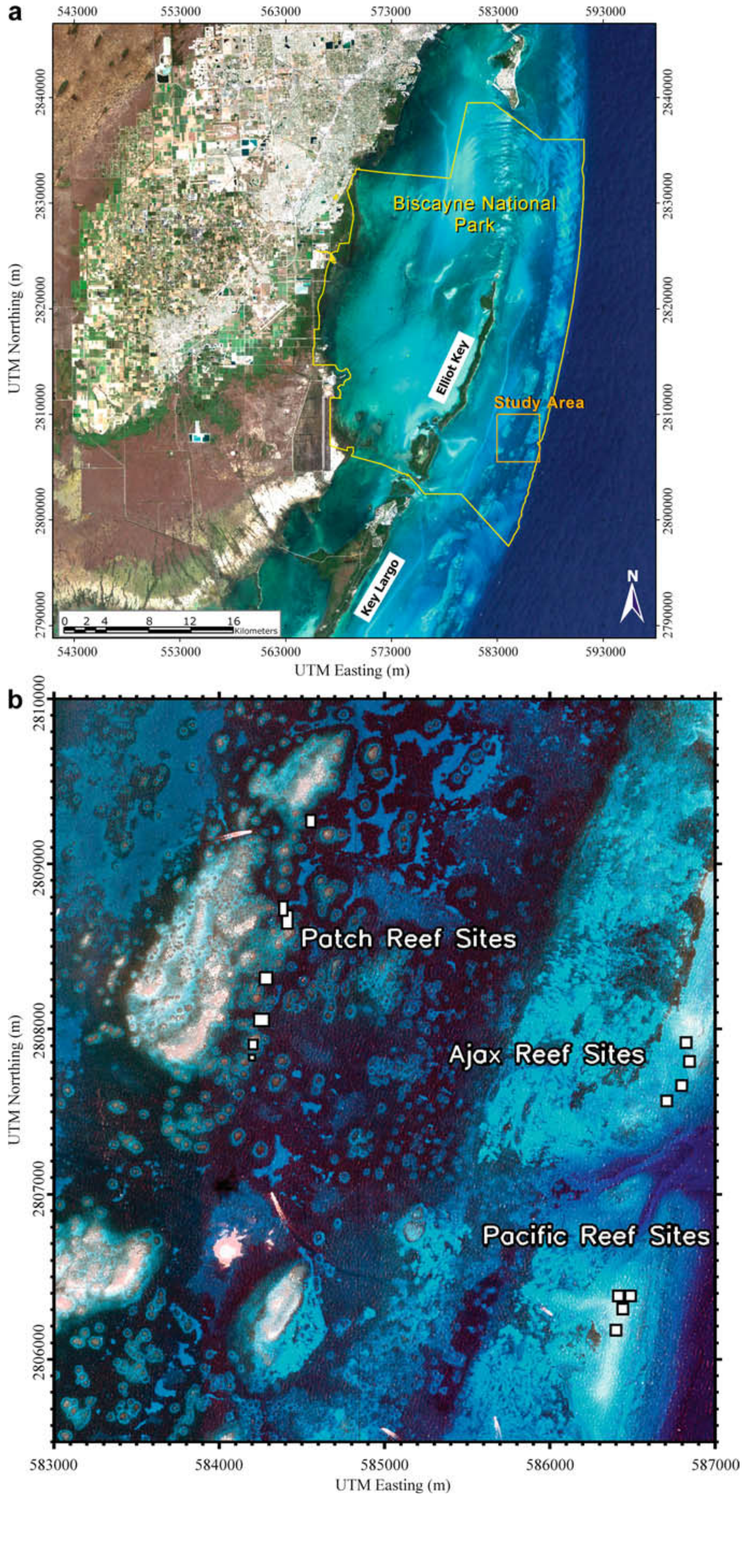

Fig. 2 **a** Landsat satellite image map depicting the location of the study area within the northern Florida Keys reef tract. **b** QuickBird satellite image map of the study area depicting optical rugosity analysis sites. Image courtesy of Digital Globe

The abundant patch reefs in between the shelf edge and Elliott Key occur amid unconsolidated calcareous sediment. Mostly found between 3 and 7 km from land, these patch reefs are dome-shaped, and are typically at 2- to 9-m water depth. Within the study area, patch reefs occur as isolated domes, or in coalesced linear chains. Individual patch reef domes are roughly circular, and have a maximum vertical relief of about 3 m. Generally near 20 m in breadth, the patches range in diameter from several meters to more than 100 m. The upward growth of patch reefs in the study area is limited by sea level, and mature patch reefs normally have irregularly flat upper surfaces dominated by octocorals on top of a framework built by scleractinian corals (Jones 1977; Marszalek et al. 1977; Jaap 1984; Shinn et al. 1989).

Pacific Reef and Ajax Reef, the outer bank reefs within the study area, are among the northernmost members of a discontinuous chain of shelf-margin reefs that extends from the Dry Tortugas to Fowey Rocks just south of Miami. The shallow reef flats of these bank-barrier reefs form the shallow shelf edge at 5- to 10-m depth. Dead encrusted *Acropora palmata* skeletons and rubble dominate the reef flat. Pacific Reef and Ajax Reef both lack the seaward spur-and-groove structure and the ocean-facing *Acorpora palmata* fringe that is observed on outer bank reefs to the south (Marszalek et al. 1977; Japp 1984; Shinn et al. 1989).

Advent of submarine topographic LIDAR

Laser-ranging devices that can measure distances in excess of 2,000 m at accuracies of better than 3 cm have been available for several decades. However, high-performance airborne laser scanning of *subaerial* topography did not become possible until the capability to very accurately determine aircraft position was provided by kinematic differential GPS methods in the early 1990s (Ackermann 1999). The ongoing rapid development of operational airborne topographic LIDAR systems for dry land applications quickly followed (Fowler 2001).

Most topographic LIDAR for land surveys are designed for the automated creation of digital elevation models (DEMs), and have a common basic design that is composed of four fundamental subsystems. These are (1) a pulsed laser transmitter/receiver, (2) GPS receivers, (3) an inertial measurement unit (IMU) for platform-attitude determination, and (4) an opto-mechanical scanner (Wehr and Lohr 1999). Topographic LIDARs typically employ a tightly focused (beam divergence ~0.25 to 2 mrad), low-energy (~100 μJ), eye-safe, high pulse repetition frequency (5 to 80 kHz), *near-infrared* wavelength (1,064 nm) laser transmitter for aircraft-to-ground range determination. The time history of the instantaneous aircraft position throughout a survey flight is determined to an XYZ coordinate accuracy of about 5 to 7 cm (Fowler 2001). This high-precision aircraft positioning is accomplished through kinematic differential GPS techniques that use the difference in the dual frequency (L1 and L2) carrier phase-derived ranges determined for both the aircraft and a nearby ground base station (Krabill and Martin 1987). At an altitude typically near 1,000 m, an opto-mechanical scanner deflects the laser across the aircraft ground track. Together with the forward aircraft velocity (~50 m/s), the scanner creates a swath of elevation measurements, usually in either a raster or an elliptical pattern (Wehr and Lohr 1999).

Interest in the role of moderate to high biomass forests in global biogeochemistry has driven the recent development of a subset of LIDARs for subaerial surveys that can provide three-dimensional, volumetric information on vegetation canopy structure (Means et al. 1999; Harding et al. 2001). Rather than providing only one or two range measurements for each laser pulse (Fowler 2001), instruments such as the Scanning Lidar Imager of Canopies by Echo Recovery (SLICER) and the Laser Vegetation Imaging Sensor (LVIS) record the time-resolved laser pulse backscatter from throughout the canopy to the underlying dry land surface (Blair and Hofton 1999). This design characteristic—the capture of the temporal reflection history for individual laser pulses—is a fundamental aspect of the EAARL approach to measuring *submarine* topography using a single *green* wavelength laser (Wright and Brock 2002).

The point elevation datasets produced by topographic LIDAR systems are inherently georeferenced, with vertical and horizontal root mean square errors of 15 cm and 10 to 100 cm, respectively (Fowler 2001). Unlike the measurements provided by traditional *bathymetric* LIDARs, these topographic soundings are geopositioned vertically in relation to the constellation of GPS satellites, requiring no Earth-reference surface. The resulting ground elevations are usually converted to a mean sea-level datum by the use of a geoid model in post-processing (Krabill et al. 2000). Laser surface footprints typically range from 0.25 to 2 m in diameter, and can exceed one spot per square meter in spatial density (Fowler 2001). In contrast to passive remote sensing, topographic LIDAR (active remote sensing) surveys may be conducted at night or below overcast skies. The inherent absolute georeferencing, small laser spot footprints, and extremely high spatial density of subaereal topographic LIDARs are highly desirable characteristics for investigation of coral reef ecosystems. However, the *near-infrared* operating wavelength of these instruments affords no significant penetration of the water column, and renders this class of LIDARs unsuitable for mapping shallow benthic substrates.

The EAARL has close affinities to the subset of topographic LIDARs engineered to sense the vertical structure of vegetation canopies (Table 1). In common with vegetation canopy LIDARs, the EAARL uses a temporal waveform-resolving, laser transmitter–receiver (Lefsky et al. 1999). However, the EAARL uses a *green* wavelength (532 nm) laser to enable water penetration and the surveying of shallow benthic substrates, similar to traditional bathymetric LIDARs designed for water depth sounding (Guenther 2001). In other design aspects, the EAARL differs fundamentally from traditional high beam divergence (~2 m ground spot diameter), low pulse repetition frequency (< 1,000 Hz) bathymetric LIDARs that typically use a second near-infrared (1,064 nm) laser to sound the water surface for vertical spot positioning (Guenther 2001). In contrast, the EAARL employs a low beam divergence (< 20 cm ground spot diameter), high pulse repetition frequency (up to 10,000 Hz) laser mounted on an aircraft platform whose position is determined by carrier phase kinematic differential GPS techniques. This hybrid design enables high spatial resolution observations of both *subaerial* and shallow *submarine* topography (Wright and Brock 2002).

The NASA EAARL is composed of four basic components: (1) a temporal waveform-resolving, pulsed laser altimeter, (2) GPS carrier phase tracking receivers, (3) a system for the determination of aircraft attitude, and (4) a raster scanner (Fig. 1). The EAARL laser transmitter is a Continuum EPO-5000 frequency-doubled YAG laser that produces up to 10,000 1.3-ns duration, 70-μJ, 532-nm wavelength pulses each second. The EAARL transmitter pulse repetition frequency is varied along each across-track raster scan in order to produce nearly equal cross-track sample spacing and near-uniform sample density within the EAARL swath. Each reflected pulse (see below) is captured simultaneously by four high-speed temporal waveform digitizers connected to four sub-nanosecond photo-detectors that vary in brightness sensitivity. The parallel operation of these four variably sensitive photo-detectors allows cross-environment surveys that include abrupt surface brightness boundaries, typically a cause of saturation in sensors optimized for viewing dark water targets. The temporal resolution of laser backscatter digitization is 1 ns, equivalent to 15 cm in air or 11 cm in water (Wright and Brock 2002).

Accurate geolocation of each EAARL spot requires knowledge of the aircraft attitude and geographic location in latitude, longitude, and altitude above the WGS-84 ellipsoid. The geographic location of the primary EAARL GPS antenna is measured at 10 Hz by two onboard Ashtech Euro-card GPS receivers. These kinematic GPS measurements are made relative to fixed GPS base stations sited at the departure airport and in the vicinity of the survey region. Precision attitude (pitch, roll, and heading) information is acquired from a Trimble TANS-Vector GPS-based attitude system at 10 Hz. Aircraft position provided by the GPS

Table 1 NASA EAARL system characteristics

Specification	Value
Total system weight	250 lb
Maximum power requirement	28 VDC at 26 A
Nominal surveying altitude	300 m above ground level
Nominal surveying speed	97 knot (50 m/s)
Maximum pulse repetition frequency	10,000 Hz
Raster scan rate	25 raster per second
Laser sample per raster	120
Swath width at 190-m altitude	130 m
Sample spacing at 190-m altitude (swath center)	0.8 m
Area surveyed per hour (300-m altitude, 50 m/s)	43 km^2 per hour
Nominal power required	400 W
Illuminated laser spot diameter on the surface	15 cm
Nominal ranging accuracy	Topographic: <7 cm Bathymetric: TBD
Nominal horizontal positioning accuracy	<1 m
Digitizer temporal resolution	1 nanosecond (14.9 cm in air, 11.3 cm in water)
Minimum measurable water depth	30 cm
Maximum measurable water depth	25 m

receivers is used to develop high-precision steering displays that enable the pilot to navigate the aircraft within several meters of the predetermined flight track.

The EAARL platform is a twin-engine Cessna 310 aircraft. This light aircraft can operate from paved runways as short as 1,000 m in length, transit at 180 knots between operating areas, slow to about 100 knots (~50 m/s) for survey operations, and has a maximum endurance of just over 9 h when operated at survey speed (~50 m/s) and altitude (~300 m). A single pilot and a LIDAR operator constitute the crew for most survey operations.

The EAARL system incorporates an Axis 2120 downlooking digital network camera that continuously acquires digital aerial photographs at a 1-s time step. The digital camera is co-registered to the EAARL optical system, and its 45° wide across-track field of view slightly exceeds the EAARL scan width. During recent test flights over the relatively clear waters of the Florida Keys, under the most favorable conditions, the EAARL surveyed *submarine* topography to water depths in excess of 25 m (Wright and Brock 2002). Overall, the Florida Keys flights demonstrated that the EAARL can routinely map coral reef habitats ranging in depth from 0.3 to 15 m below the water surface.

EAARL survey missions

During a 2-week time period in August 2002, EAARL missions staged from Marathon, Florida, collected dense submarine topographic measurements over the northern Florida Keys reef tract. These overflights resulted in the collection of 82 gigabytes of data, inclusive of LIDAR temporal waveform and aircraft trajectory datasets, and digital camera images. EAARL LIDAR coverage was acquired by at least two flight passes over all of a broad swath extending from north of Triumph Reef to south of Carysfort Reef. To ensure acquisition of dense LIDAR coverage for optical rugosity analysis, the missions on 4 August and 5 August each repeated a single flightline positioned to survey bank reefs and patch reefs, respectively. The shelf-edge flightline over bank reefs was flown 10 times between fixed north (UTM zone 17 easting: 588,960 m, northing: 2,817,080 m) and south (UTM zone 17 easting: 585,310 m, northing: 2,802,740 m) waypoints. The landward patch reef flightline was parallel, followed the seaward flank of Anniversary Reef, and was flown nine times (north waypoint: UTM zone 17 easting 586,445 m, northing 2,817,230 m; south waypoint: UTM zone 17 easting 583,000 m, northing 2,803,260 m).

Data processing

Recent underwater video and belt transect monitoring by Moulding and Patterson (2002) provided quantitative descriptions of benthic cover, and coral species richness and diversity on patch, bank, and transitional reefs within the study area. Five sites were picked for optical rugosity analysis (ORA) to match these sites of recent monitoring. The remainder of the 15 ORA sites was selected by inspection of January 2001 AISA airborne hyperspectral imagery and a QuickBird satellite image acquired in April 2002. In the configuration used for the BNP survey, the AISA is a hyperspectral sensor that provides georeferenced 1.5-m-resolution imagery in 26 10-nm-wide spectral channels from an operating altitude of 1,500 m (Oliver Weatherbee, personal communication). The QuickBird satellite is operated by DigitalGlobe Inc., and provides 2.44-m (nadir) resolution multispectral geolocated imagery in four spectral channels (DigitalGlobe 2002). Each of the ORA sites was assigned a site identifier composed of its UTM centerpoint coordinates, followed by the UTM zone number (Table 2).

The patch reef sites (Fig. 3a; Table 2) vary in area to match the east–west and north–south patch dimensions (Fig. 2b). The bank reef sites (Fig. 3b; Table 2) are all 50-m-wide square areas on either north Pacific Reef or south Ajax Reef (Fig. 2b; Table 2). One patch reef site covering Alina Reef (e584207_n2807950_17) and one bank reef site on Pacific Reef (e586343_n2806350_17) were selected to illustrate various measures of optical rugosity.

In the present paper, an "ORA transect" is equivalent to a single EAARL raster scan across the aircraft ground flight track. At each site, all of the ORA transects acquired on either 4 August 2002 (bank reefs) or 5 August 2002 (patch reefs) were extracted from the full EAARL dataset for that mission. The 190-m aircraft altitude maintained during the missions on 4–5 August 2002 resulted in roughly 130-m-long ORA transects composed of 20-cm surface-diameter laser spots with a nominal substrate spacing of approximately 0.8 m. Elevation-threshold filters were applied to each transect to eliminate LIDAR waveforms that lacked a significant bottom reflection, or did not fall on a reef substrate (Table 3).

The filtered LIDAR temporal waveform datasets were next processed to create a voluminous set of submarine topographic transects for each ORA analysis site, referenced to the NAVD88 vertical datum and the NAD83 horizontal datum (Fig. 4a). This step involved the use of algorithms that examine each temporal waveform (Fig. 5) to determine the range to the sea surface and the water-column thickness. The absolute horizontal positioning accuracy for each spot elevation point is approximately 1 m, and the absolute vertical accuracy is approximately 15 cm (Wright and Brock 2002). The relative horizontal point-positioning precision, highly significant to the analysis of topographic complexity presented below, is on the order of 10 cm or less.

Optical indices of topographic complexity

At every site, each ORA transect (Fig. 4a) was evaluated separately within an analysis of topographic complexity. The first step in the analysis of a given transect was the determination of the direct geometric distance (D_{geom}) between each geolocated elevation point along the transect and the western geolocated elevation endpoint of the transect (Fig. 4b). Second, the transect surface contour-following distance (D_{tran}) between each point along the transect and the western endpoint of the transect was calculated

Table 2 Specifications for the optical rugosity analysis sites. Alina Reef and Pacific Reef sites selected to illustrate the analysis are shown in *italics*

Site type	Site name	Site identifier	NAVD88 elevation range (m)	Minimum easting (m)	Maximum easting (m)	Minimum northing (m)	Maximum northing (m)
Patch reef	Not named	e584151_n2807732_17	−5.0 to 0.0	584,141	584,161	2,807,721	2,807,743
Patch reef	Not named	e584157_n2807806_17	−5.0 to 0.0	584,138	584,176	2,807,785	2,807,827
Patch reef	*Alina Reef*	*e584207_n2807950_17*	*−5.0 to 0.0*	*584,170*	*584,245*	*2,807,920*	*2,807,980*
Patch reef	Not named	e584231_n2808190_17	−5.0 to 0.0	584,202	584,261	2,808,160	2,808,220
Patch reef	Not named	e584356_n2808532_17	−5.0 to 0.0	584,331	584,381	2,808,485	2,808,580
Patch reef	Not named	e584332_n2808596_17	−5.0 to 0.0	584,315	584,350	2,808,561	2,808,631
Patch reef	Not named	e584490_n2809103_17	−6.0 to −1.0	584,470	584,510	2,809,073	2,809,133
Bank reef	Pacific Reef	e586273_n2806350_17	−6.0 to −1.0	586,248	586,298	2,806,325	2,806,375
Bank reef	*Pacific Reef*	*e586343_n2806350_17*	*−6.0 to −1.0*	*586,318*	*586,368*	*2,806,325*	*2,806,375*
Bank reef	Pacific Reef	e586300_n2806275_17	−6.0 to −1.0	586,275	586,325	2,806,250	2,806,300
Bank reef	Pacific Reef	e586260_n2806150_17	−6.0 to −1.0	586,235	586,285	2,806,125	2,806,175
Bank reef	Ajax Reef	e586554_n2807480_17	−7.0 to −2.0	586,529	586,579	2,807,455	2,807,505
Bank reef	Ajax Reef	e586685_n2807710_17	−7.0 to −2.0	586,660	586,710	2,807,685	2,807,735
Bank reef	Ajax Reef	e586665_n2807820_17	−7.0 to −2.0	586,640	586,690	2,807,795	2,807,845
Bank reef	Ajax Reef	e586641_n2807569_17	−7.0 to −2.0	586,616	586,666	2,807,544	2,807,594

Fig. 3 **a** Underwater photograph depicting the substrate at a patch reef just to the north of Alina Reef. **b** Underwater photograph depicting the substrate at north Pacific Reef

(Fig. 4b). Third, at each point along the transect, the partial-transect optical rugosity (Ro_{part}, dimensionless) was calculated as (Fig. 4c):

$$R_{Opart} = \frac{D_{tran}}{D_{geom}} \quad (1)$$

By definition, Ro_{part} must always be greater than or equal to 1. For a perfectly flat, smooth surface, the value of this ratio is 1. Higher values of this ratio correspond to greater departure from smooth flatness. Fourth, the optical rugosity assigned to the entire transect (Ro_{tran}) was set equal to the peak partial-transect rugosity obtained for that transect (Fig. 4c):

$$R_{Otran} = \max\left(R_{Opart}\right) \quad (2)$$

This selection of the maximum optical rugosity attained along the transect was adopted in order to capture the highest level of topographic complexity that was sensed within the site by the associated LIDAR raster scan. Note that a simple average of optical rugosity over the entire transect would suppress the recognition of high rugosity segments along transects that are otherwise flatter.

Next, at each point along a given transect, the elevation difference relative to the adjacent point closer to the transect origin point was calculated (δE_{ap}, length dimension; Fig. 4d). Finally, the absolute values of the resulting elevation differences were used to calculate the average adjacent point elevation change, Av(δE_{ap}), for each transect.

To allow the comparison of topographic complexity between sites taken as a whole, the *whole-site* mean and maximum values of Ro_{tran} and Av(δE_{ap}) for the entire population of ORA transects at each site, along with their standard deviations, were calculated. Ro_{tran} and Av(δE_{ap}) are both optical indices of topographic complexity. As determined by our procedures described above, Ro_{tran} provides a measure of the extreme in topographic complexity attained over the entire length of each transect, and Av(δE_{ap}) captures the topographic variability between immediately adjacent points.

Results

The point datasets collected for all sites were first filtered to remove false bottom returns due to laser reflection within the water column or atmosphere. After the application of an elevation threshold to filter out points that did not fall upon a reef substrate, the patch

Table 3 Characteristics of the filtered LIDAR datasets extracted for the optical rugosity analysis sites. Alina Reef and Pacific Reef sites selected to illustrate the analysis are shown in*italics*

Site name	Site identification number	Pre-filtering analysis area (m^2)	Post-filtering analysis area (m^2)	Total number of LIDAR transects	Total number of points	Point density (points/m^2)
Not named	e584151_n2807732_17	440.0	286.4	36	530	1.85
Not named	e584157_n2807806_17	1,596.0	1,174.1	76	1,867	1.59
Alina Reef	*e584207_n2807950_17*	*4,500.0*	*3,658.5*	*121*	*4,396*	*1.20*
Not named	e584231_n2808190_17	3,540.0	2,747.3	97	1,985	0.72
Not named	e584356_n2808532_17	4,750.0	3,958.0	194	4,986	1.26
Not named	e584332_n2808596_17	2,450.0	2,119.5	70	1,261	0.59
Not named	e584490_n2809103_17	2,400.0	2,135.9	43	824	0.39
Pacific Reef	e586273_n2806350_17	2,500.0	2,208.0	163	4,727	2.14
Pacific Reef	*e586343_n2806350_17*	*2,500.0*	*2,223.0*	*143*	*3,646*	*1.64*
Pacific Reef	e586300_n2806275_17	2,500.0	2,220.0	170	5,181	2.33
Pacific Reef	e586260_n2806150_17	2,500.0	2,218.0	168	5,425	2.45
Ajax Reef	e586554_n2807480_17	2,500.0	2,272.0	159	4,713	2.07
Ajax Reef	e586685_n2807710_17	2,500.0	2,201.0	137	3,277	1.49
Ajax Reef	e586665_n2807820_17	2,500.0	2,309.0	175	5,638	2.44
Ajax Reef	e586641_n2807569_17	2,500.0	2,264.0	148	4,439	1.96

reef sites varied in analysis area from 286.4 to 3,958.0 m^2 (Table 3). Elevation filtering to remove points that fell on non-reef substrates was not applied to the bank reef sites, because all of these sites are wholly contained within the boundaries of either Pacific Reef or Ajax Reef. Although all of the bank reef sites are 50 m square, following the ''false bottom'' filtering step, they varied in analysis area from 2,201.0 to 2,309.0 m^2 (Table 3). The area point density for patch reef sites ranged from 0.39 to 1.85 points per m^2, and at bank reef sites this value varied between 1.49 and 2.45 points per m^2. Given that the bank reef sites are in slightly deeper water than the patch reefs, the higher resultant point density on bank reefs was unexpected. Possible explanations for this result are that the bank reef flightline was overflown 10 times versus the nine overpasses of the patch reef flightline, and in addition, the relative brightness of the bank reefs may have facilitated laser sounding.

The optical rugosity analysis revealed a distinct pattern of variation in whole-site ORA measures of topographic complexity between bank reef and patch reef sites (Table 4). Three groupings of sites—Pacific Reef sites, Ajax Reef sites, and patch reef sites—are clearly evident along a curvilinear trend on a plot of whole-site mean Ro_{tran} versus whole-site mean $Av(\delta E_{ap})$ (Fig. 6). The Pacific Reef sites form a tight cluster, ranging in whole-site mean $Av(\delta E_{ap})$ from 0.1085 to 0.1165, and from 1.0153 to 1.0172 in whole-site mean Ro_{tran}. The south Ajax Reef sites plot close to the Pacific Reef cluster along a trend toward greater topographic variability, revealing subtle morphological differences between these quite similar bank reef regions. Aside from Alina Reef, the site with the highest mean Ro_{tran} (1.1023), all of the patch reef sites fall along a near-linear trend on the whole-site mean Ro_{tran} versus whole-site mean $Av(\delta E_{ap})$ plot (Fig. 6). Patch reef sites vary widely in whole-site mean Ro_{tran} and $Av(\delta E_{ap})$, from 1.0385 to 1.1023 and from 0.1727 to 0.2521 m, respectively.

An analogous pattern of variation between bank and patch reefs is evident on a plot of the standard deviation of whole-site mean Ro_{tran} versus the standard deviation of whole-site mean $Av(\delta E_{ap})$ (Fig. 7). Both the north Pacific Reef and south Ajax Reef sites form clusters at low relative standard deviation of both measures of topographic complexity, with variability in Ro_{tran} slightly higher at Ajax Reef. Again, all but one of the patch reef sites fall along a rough trend line toward higher internal-site variability in both Ro_{tran} and $Av(\delta E_{ap})$. Plots of transect Ro_{tran} versus $Av(\delta E_{ap})$ for Alina Reef and a Pacific Reef site (e584207_n2807950_17, e586343_n2806350_17; Fig. 8a, b) illustrate the higher internal-site variability in transect topographic complexity at patch reef sites relative to bank reef sites.

Discussion

Optical rugosity of patch and bank reef communities

Patch reefs in the study area are host to a varied assemblage of scleractinian corals, octocorals, sponges, invertebrates, and algae. Some of these reefs are formed of single enormous colonies of *Montastrea annularis*, and, in general, display wide variability in coral abundance, density, and diversity. Mature patch reefs have a characteristic zonation, with large *Montastrea annularis* and *M. cavernosa* heads developed on the seaward eastern and southeastern margins (Jones 1977). Typically, *Diploria* and *Colpophyllia* heads over 1 m wide preferentially occur in the lee of the *Montastrea* heads, and scattered smaller *Siderastrea* heads occur across the patch interior and landward margins (Jones 1977). Northern Florida Keys patch reefs are sites of intense recruitment and high coral mortality, and across the interior of mature patches, octocorals appear to competitively exclude stony corals (Jones 1977; Marszalek

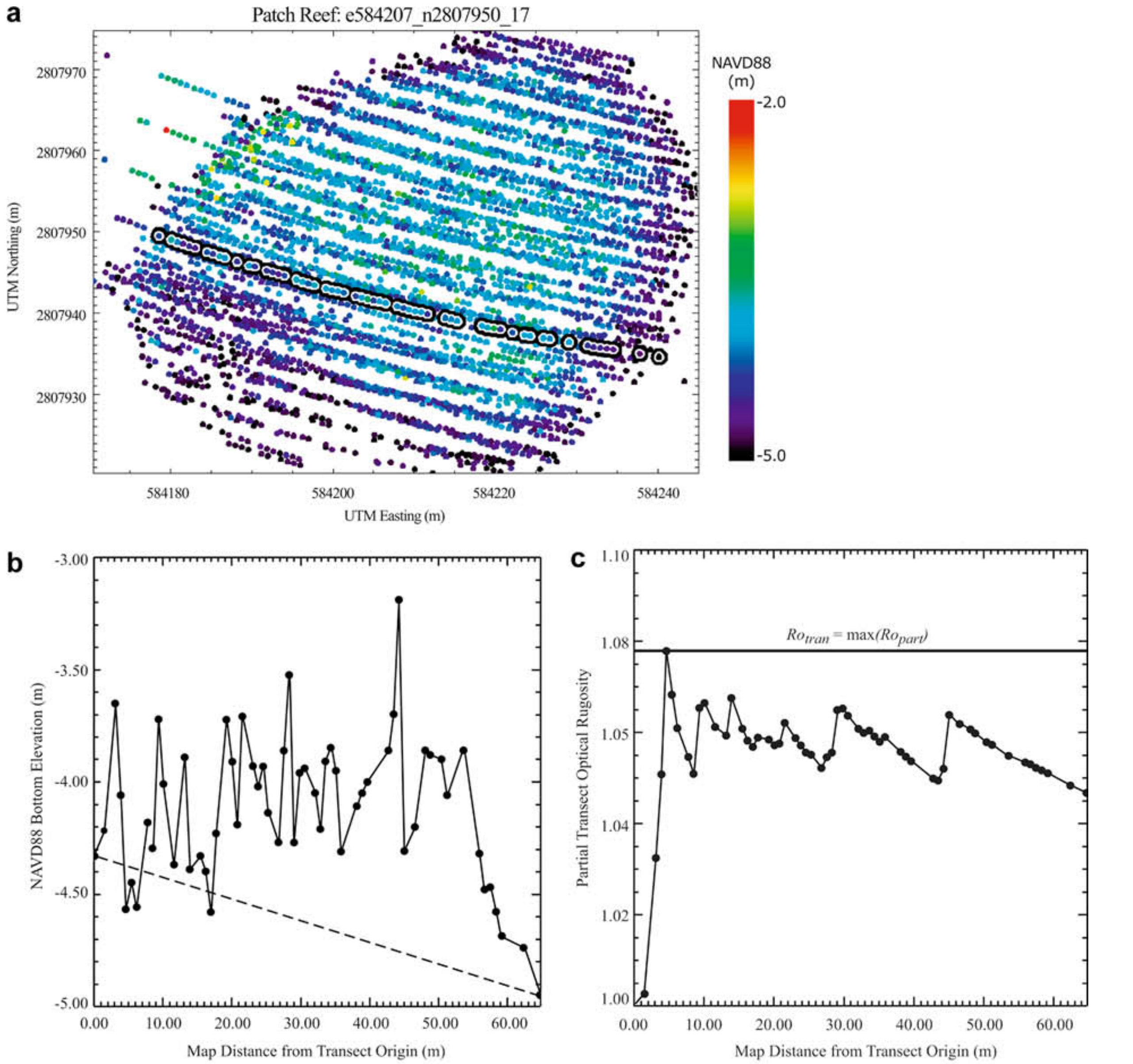

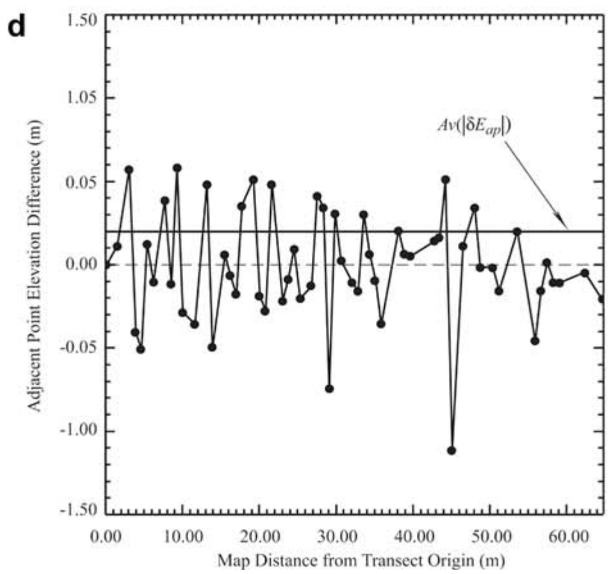

Fig. 4a–d Illustration of the optical rugosity analysis performed on each LIDAR transect. **a** Map depicting color-coded spot NAVD88 referenced elevations over Alina Reef (*highlighted spots* populate the LIDAR raster transect selected to demonstrate the analysis). **b** Submarine topographic transect based on selected LIDAR raster. The distance along the *dashed line* is equivalent to D_{geom} between the two endpoints, and the distance along the *solid line* is equivalent to D_{tran}. **c** Local point partial-transect rugosity transect based on selected LIDAR raster. The value for transect optical rugosity is defined as the peak value attained by the partial-transect optical rugosity. **d** Adjacent point elevation difference transect based on selected LIDAR raster

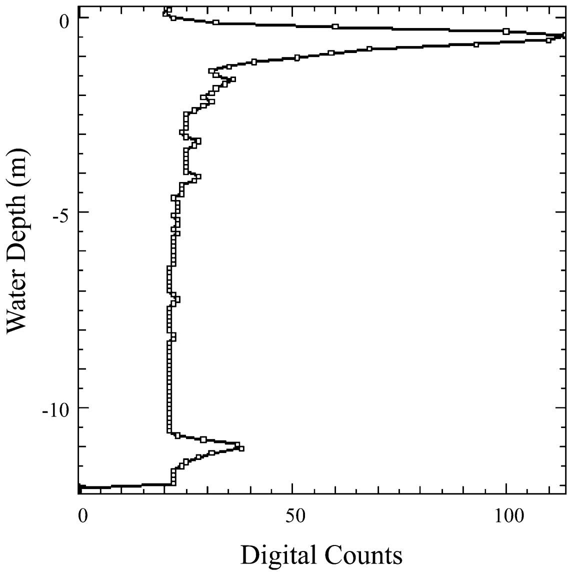

Fig. 5 A reflected LIDAR waveform collected within the Florida Keys reef tract at UTM zone 17 easting 588,185.6 m, northing 2,812,502.7 m, on 6 September 2001. The water-column thickness based on this waveform is estimated to be 11.7 m

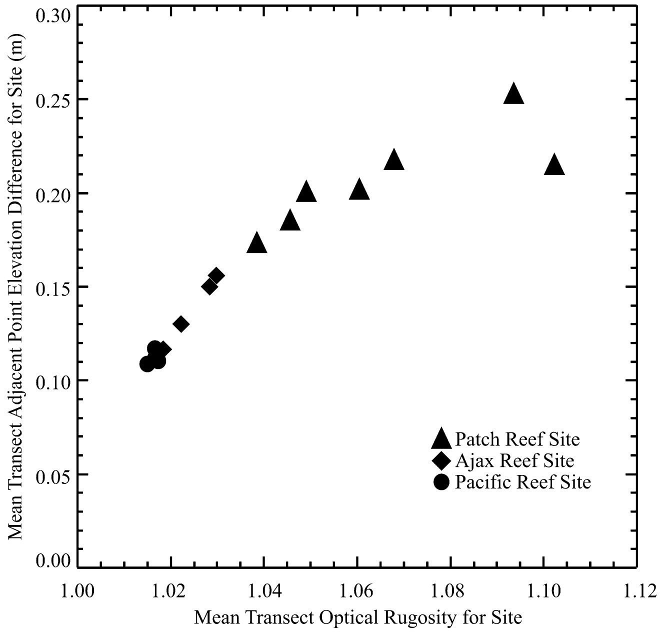

Fig. 6 Scatterplot of site mean transect rugosity vs. site mean transect point-to-point elevation difference for all sites. Each *dot* represents an analysis site

et al. 1977; Japp 1984; Shinn et al. 1989; Miller et al. 2000).

Inspection of a digital elevation model (DEM) of Alina Reef (site e584207_n2807950_17) reveals that this typical patch reef community results in topographic detail that is sensed by EAARL LIDAR scanning (Fig. 9). On this patch reef, and on many others that we have examined, features revealed by the LIDAR survey include the overall patch geomorphology, the steepness of patch edges, and holes as small as 1 m in diameter. Variable roughness across the top of this and other mid-platform patch reefs, apparently due to their resident varied assemblage of scleractinian corals, octocorals, sponges, invertebrates, and algae, is also clearly evident on EAARL-derived DEMs.

Recent benthic assessments have revealed that, Florida Keys-wide, live coral cover on some patch reefs reaches nearly 28% (Miller et al. 2002). These sites exhibit some of the highest present-day coral cover in the Florida Keys, contain the greatest coral species richness found throughout the reef tract, and are particularly diverse in gorgonian species (Miller et al. 2002). In spite of their proximity to Caesar's Creek, a source of chilled, turbid bay waters in winter, patch reefs in the study area are significantly higher in coral cover and richness than are the seaward bank reefs (Burns 1985; Miller et al. 2000). Recent assessments by Moulding and Patterson (2002) found mean stony and mean octocoral cover on these patch reefs in excess of 8 and 35%, respectively.

Table 4 Results of the optical rugosity analysis. Alina Reef and Pacific Reef sites selected to illustrate the analysis are shown in *italics*

Site type	Site name	Site identification number	Site mean Av(δE_{ap}) (m)	Site mean Ro_{tran}
Patch reef	Not named	e584151_n2807732_17	0.1842	1.0456
Patch reef	Not named	e584157_n2807806_17	0.1998	1.0492
Patch reef	*Alina Reef*	*e584207_n2807950_17*	*0.2143*	*1.1023*
Patch reef	Not named	e584231_n2808190_17	0.2521	1.0937
Patch reef	Not named	e584356_n2808532_17	0.2008	1.0605
Patch reef	Not named	e584332_n2808596_17	0.1727	1.0385
Patch reef	Not named	e584490_n2809103_17	0.2168	1.0679
Bank Reef	Pacific Reef	e586273_n2806350_17	0.1165	1.0167
Bank reef	*Pacific Reef*	*e586343_n2806350_17*	*0.1085*	*1.0153*
Bank reef	Pacific Reef	e586300_n2806275_17	0.1147	1.0169
Bank reef	Pacific Reef	e586260_n2806150_17	0.1104	1.0172
Bank reef	Ajax Reef	e586554_n2807480_17	0.1499	1.0284
Bank reef	Ajax Reef	e586685_n2807710_17	0.1165	1.0183
Bank reef	Ajax Reef	e586665_n2807820_17	0.1302	1.0222
Bank reef	Ajax Reef	e586641_n2807569_17	0.1557	1.0298

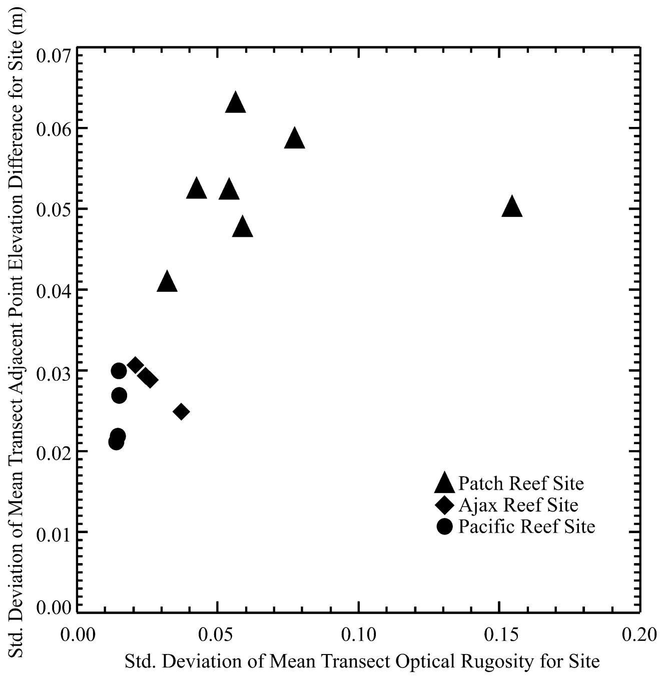

Fig. 7 Scatterplot of the standard deviation of peak transect rugosity vs. the standard deviation of transect mean point-to-point elevation difference for all sites

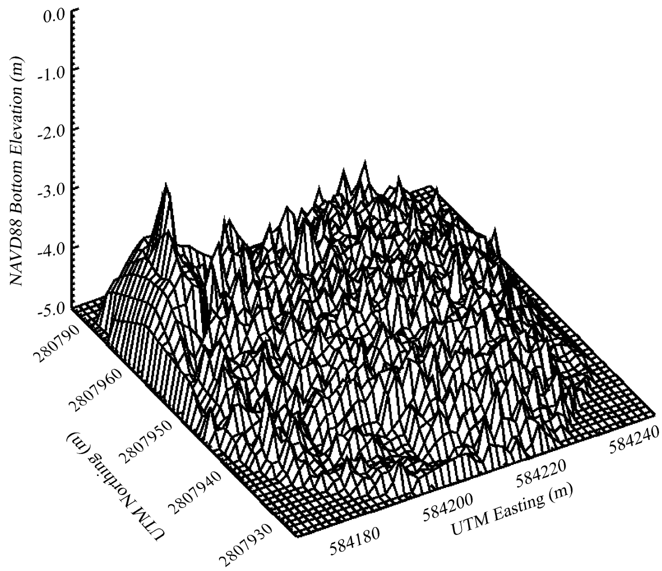

Fig. 9 Wire mesh plot depicting a digital elevation model created for Alina Reef (site e584207_n2807950_17) based upon the NASA EAARL survey that was conducted on 5 August 2002. The viewing angle is oblique and from the southwest

Pacific Reef and Ajax Reef were built mainly by *Acropora palmata* colonies that have since died (Shinn et al. 1989), and are now depauperate of all species of living reef corals in their shallow zones (Miller et al. 2000). Essentially, these outer bank reefs are limestone ridges capped by a thin, scattered veneer of live corals and other reef organisms, but below 12 m there is more abundant living coral growth on antecedent reef platforms (Jaap 1984). The dominant benthic macrobiota on the shallow reef-flats are scattered small *Porites* and *Siderastrea* heads, encrusting *Millepora* coral, echinoids, sponges, and the calcareous benthic alga *Halimeda opuntia*. Large coral colonies are virtually absent from the shallow zone of these offshore reefs (Miller et al. 2000). All of the BNP bank reefs assessed by Moulding and Patterson (2002) had less than 2% mean stony coral cover, and mean octocoral cover below 20%. Alina Reef (patch reef) and Pacific Reef (bank reef), the ORA demonstration sites, illustrate the consistently

Fig. 8a, b Scatterplots of transect mean point-to-point elevation difference vs. transect rugosity for selected sites: **a** Alina Reef (site e584207_n2807950_17), and **b** Pacific Reef (site e586313_n2806347_17). Each *dot* represents a single ORA transect

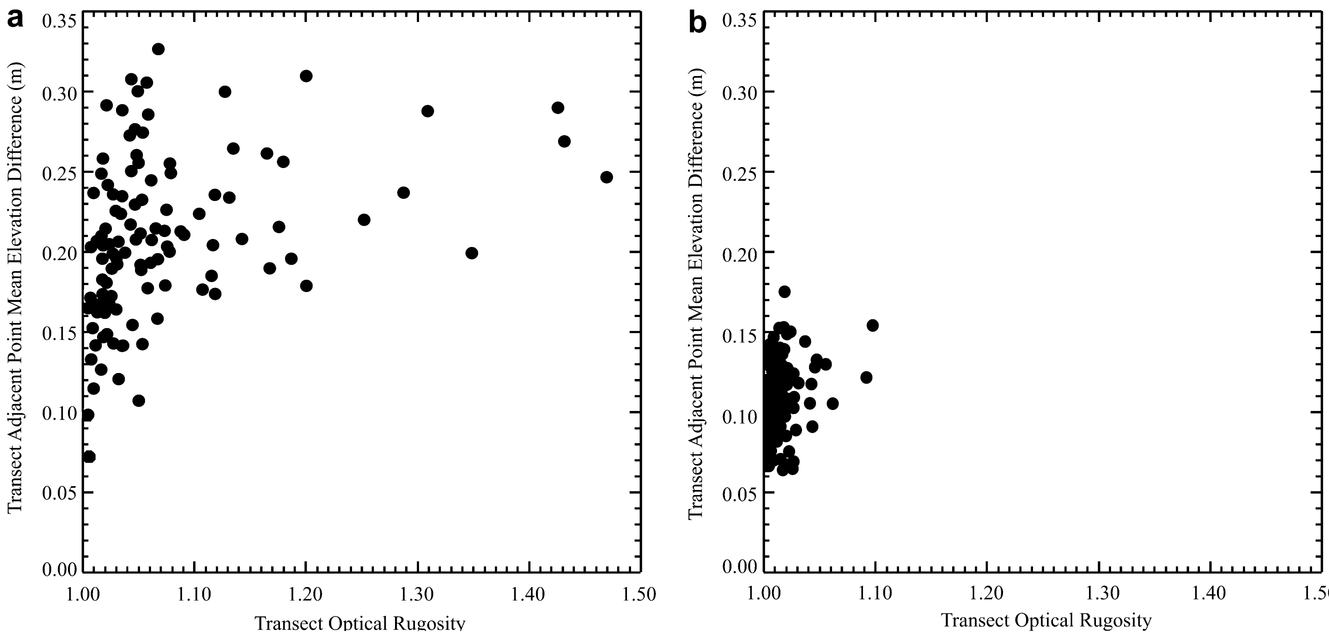

higher coral density, species richness, and diversity on BNP patch reefs versus bank reefs described by Moulding and Patterson (2002) (Fig. 3).

Measures of optical rugosity (Figs. 6, 7 and 8, and Table 4) indicate that the previously recognized (Burns 1985; Miller et al. 2000, Moulding and Patterson 2002) higher habitat complexity of lagoonal patch reefs versus outer bank reefs results in a parallel gradient in topographic complexity that can be sensed by the EAARL. Further, the internal variability of topographic complexity as observed by this instrument is higher at patch reefs compared to outer bank reefs. This result suggests a more heterogeneous habitat at the mid-shelf patch reefs. Although the sets of bank reef sites at Pacific Reef and Ajax Reef are quite similar in LIDAR measures of morphologic variability, significant variation in optical rugosity was found among the patch reef sites. This variation in patch reef optical rugosity may be due to framework structure differences, age, and associated changes in coral cover or assemblage, or variability in recent natural or anthropogenic impacts. At the bank reef sites, rugosity-forming corals, such as *Acropora palmata*, are nearly all dead, and their skeletons have eroded, yielding low rugosity, which is adequately represented by the LIDAR-based index. Although explanation of the origin of variation in the LIDAR-resolved topographic complexity of BNP patch reefs is outside the scope of this paper, we plan to undertake an investigation of this topic.

Conclusions

Optical rugosity analysis revealed variation in whole-site measures of LIDAR-sensed topographic complexity that matches previous in-situ qualitative and belt-transect assessments of the relative habitat complexity of bank reefs and patch reefs in the study area. The EAARL measured higher whole-site optical indices of topographic variability at patch reefs relative to bank reefs, which was consistent with field observations of higher stony coral cover, octocoral cover, and coral species richness on patch reefs relative to the rubble-dominated bank reefs within the study area. Since LIDAR optical rugosity measurements clearly reflected key benthic parameters, it has potential application as a monitoring tool capable of detecting changes in reefs over large areas.

Acknowledgements The USGS Coastal and Marine Geology Program funded this investigation as a component of the Geologic Studies of Coral Reefs Project. The authors greatly appreciate substantial contributions from R. Curry and S. Viehman to the field investigations within Biscayne National Park. The authors thank D. Hickey and B.J. Reynolds for their professionalism in handling the boat operations undertaken within this study. B. Boynton and M. Harris are gratefully acknowledged for assistance in the preparation of figures. V. Rabine is thanked for his dedication and skill as the Chief Pilot of the Cessna 310 aircraft used for the NASA EAARL LIDAR overflights of the northern Florida Keys reef tract.

References

Ackermann F (1999) Airborne laser scanning—present status and future expectations. J Photogram Rem Sens 54:64–67

Aronson RB, Edmunds PJ, Precht WF, Swanson DW, Levitan DR (1994) Large scale, long-term monitoring of Caribbean coral reefs: simple, quick, inexpensive techniques. Atoll Res Bull 421:1–19

Blair JB, Hofton MA (1999) Modeling laser altimeter return waveforms over complex vegetation using high resolution elevation data. Geophys Res Lett 26(16):2509–2512

Burns TP (1985) Hard-coral distribution and cold-water disturbances in South Florida: variation with depth and location. Coral Reefs 4:117–124

Chapman MR, Kramer DL (1999) Gradients in coral reef fish density and size across the Barbados Marine Reserve boundary: effects of reserve protection and habitat characteristics. Mar Ecol Prog Ser 181:81–96

DigitalGlobe (2002) QuickBird Imagery Products—product guide. DigitalGlobe Inc, Longmont

Dustan P (1999) Coral reefs under stress: sources of mortality in the Florida Keys. Nat Resources Forum 23:147–155

Edinger EN, Risk MJ (2000) Reef classification by coral morphology predicts coral reef conservation value. Biol Conserv 92:1–13

Fowler R (2001) Topographic lidar. In: Maune DF (ed) Digital elevation model technologies and applications: the DEM users manual. Soc Photogram Rem Sens, Bethesda, pp 207–236

Friedlander AM, Parrish JD (1998) Habitat characteristics affecting fish assemblages on a Hawaiian coral reef. J Exp Mar Biol Ecol 224:1–30

Ginsburg RN, Shinn EA (1994) Preferential distribution of reefs in the Florida reef tract: the past is the key to the present. In: Ginsburg RN (ed) Global aspects of coral reefs, health, hazards, and history. University of Miami, Coral Gables, pp H21–H26

Guenther GC (2001) Airborne lidar bathymetry. In: Maune DF (ed) Digital elevation model technologies and applications: the DEM users manual. Soc Photogram Rem Sens, Bethesda, pp 236–306

Harding DJ, Lefskey MA, Parker GG, Blair JB (2001) Laser altimetry canopy height profiles—methods and validation for closed-canopy, broadleaf forests. Rem Sens Environ 76:283–297

Hixon MA, Beets JP (1993) Predation, prey-refuges, and the structure of coral-reef fish assemblages. Ecol Monogr 63(1):77–101

Hudson JH, Hanson KJ, Halley RB, Kindinger JL (1994) Environmental implications of growth rate changes in *montastrea annularis*: Biscayne National Park. Bull Mar Sci 54(3):647–669

Japp WC (1984) The ecology of the south Florida coral reefs: a community profile. US Fish Wildlife Service Rep FWS/OBS-82/08

Johannes RE, Wiebe WJ, Crossland CJ, Rimmer DW, Smith SV (1983) Latitudinal limits of coral reef growth. Mar Ecol Prog Ser 11:105–111

Jones JA (1977) Morphology and development of southeastern Florida patch reefs. In: Proc 3rd Int Coral Reef Symp, University of Miami, Miami, pp 232–235

Krabill WB, Martin CF (1987) Aircraft positioning using global positioning system carrier phase data. Navigation 34:1–21

Krabill WB, Wright CW, Swift RN, Frederick EB, Manizade SS, Yungel JK, Martin CF, Sonntag JG, Duffy M, Hulslander W, Brock JC (2000) Airborne laser mapping of Assateague Island National Seashore beach. Photogram Rem Sens 66(1):65–71

Lefsky MA, Harding D, Cohen WB, Parker G, Shugart HH (1999) Surface lidar remote sensing of basal area and biomass in deciduous forests of eastern Maryland, USA. Rem Sens Environ 67:83–98

Lyzenga DR (1978) Passive remote sensing techniques for mapping water depth and bottom features. Appl Optics 17(3):379–383

Marszalek DS, Babashoff G, Noel MR, Worley DR (1977) Reef distribution in south Florida. In: Proc 3rd Int Coral Reef Symp, University of Miami, Miami, pp 224–229

Mazel CH (1999) Technical issues related to coral reef remote sensing and workshop recommendations. Rep Worksh Center for Marine Conservation, 4–5 February 1999, St. Petersburg, Florida

McCormick MI (1994) Comparison of field methods for measuring surface topography and their association with a tropical reef fish assemblage. Mar Ecol Prog Ser 112:87–96

McPherson BF, Halley RB (1996) The south Florida environment: a region under stress. US Geol Surv Circ 1134

Means JE, Acker SA, Harding DJ, Blair JB, Lefsky MA, Cohen WB, Harmon ME, McKee WA (1999) Use of large-footprint scanning airborne lidar to estimate forest stand characteristics in the western Cascades of Oregon. Rem Sens Environ 67:298–308

Miller SL, Weil E, Szmant AM (2000) Coral recruitment and juvenile mortality as structuring factors for reef benthic communities in Biscayne National Park, USA. Coral Reefs 19:115–123

Miller SL, Chiappone M, Swanson DW, Vermeij M, Eaken D (2002) Rapid assessment and monitoring of coral reef habitats on the Florida Keys reef tract: quick look report: summer 2002. NOAA NURC

Moulding A, Patterson M (2002) Biscayne National Park coral reef inventory and monitoring project. Final Report. National Park Service, Homestead

Rogers CS, Miller J (2001) Coral bleaching, hurricane damage, and benthic cover on coral reefs in St. John, US Virgin Islands: a comparison of surveys with the chain transect method and videography. Bull Mar Sci 69(2):459–470

Rogers CS, Suchanek TH, Pecora FA (1982) Effects of Hurricances David and Frederic(1979) on shallow *Acropora palmata* reef communities: St. Croix, US Virgin Islands. Bull Mar Sci 32(2):532–548

Rogers CS, Garrison G, Grober R, Hillis ZM, Franke MA (1994) Coral reef monitoring manual for the Caribbean and western Atlantic. US Dept Interior, National Park Service, Virgin Islands National Park, St. John

Sale PF (1991) Habitat structure and recruitment in coral reef fishes. In: Bell SS, McCoy ED, Mushinsky HR (eds) Habitat structure, the physical arrangement of objects in space. Chapman and Hall, New York, pp 197–210

Sandidge JC, Holyer RJ (1998) Coastal bathymetry from hyperspectral water radiance. Rem Sens Environ 65:341–352

Sebens KP (1991) Habitat structure and community dynamics in marine benthic systems. In: Bell SS, McCoy ED, Mushinsky HR (eds) Habitat structure, the physical arrangement of objects in space. Chapman and Hall, New York, pp 211–234

Shinn EA, Lidz BH, Kindinger JL, Hudson JH, Halley RB (1989) Reefs of Florida and the Dry Tortugas: a guide to the modern carbonate environments of the Florida Keys and the Dry Tortugas. Int Geol Congr Field Trip Guideb T176, Am Geophys Union, Washington

Szmant AM (1997) Nutrient effects on coral reefs: a hypothesis on the importance of topographic and trophic complexity to reef nutrient dynamics. In: Proc 8th Int Coral Reef Symp 2:1527–1532

Wehr A, Lohr U (1999) Airborne laser scanning—an introduction and overview. Photogram Rem Sens 54:68–82

Wright CW, Brock JC (2002) EAARL: a lidar for mapping shallow coral reefs and other coastal environments. In: Proc 7th Int Conf Remote Sensing Marine Coastal Environment, 20–22 May 2002, Miami